(18) Ozaki, T.; Shoji, A. *Makromol. Chem., Rapid Commun.* **1982**, *3*, 157.
(19) Heitz, F.; Spach, G. *Macromolecules* **1971**, *4*, 429.
(20) Zervas, L.; Borovas, D.; Gazis, E. *J. Am. Chem. Soc.* **1963**, *85*, 3660.
(21) Blout, E. R.; Karlson, R. H. *J. Am. Chem. Soc.* **1956**, *78*, 941.
(22) Oya, M.; Seto, K.; Sato, I. *Nippon Nôgei Kagaku Kaishi* **1966**, *40*, 58.
(23) Oya, M.; Katakai, R.; Uno, K.; Iwakura, Y. *Kôgyô Kagaku Zasshi* **1970**, *73*, 2371.
(24) Doty, P.; Bradbury, J. H.; Holtzer, A. M. *J. Am. Chem. Soc.* **1956**, *78*, 947.
(25) Pines, A.; Gibby, M. G.; Waugh, J. S. *J. Chem. Phys.* **1973**, *59*, 569.
(26) Schaefer, J.; Stejskal, E. O. *J. Am. Chem. Soc.* **1976**, *98*, 1031.
(27) Paolillo, L.; Tancredi, T.; Temussi, P. A.; Trivellone, E.; Bradbury, E. M.; Crane-Robinson, C. *J. Chem. Soc., Chem. Commun.* **1972**, 335.
(28) Bovey, F. A. *J. Polym. Sci., Macromol. Rev.* **1974**, *9*, 1.
(29) Frushour, B. G.; Koenig, J. L. *Biopolymers* **1974**, *13*, 455.
(30) This interpretation is based on a view that the ^{13}C chemical shift of *any* carbon exhibits a conformation-dependent change defined by the torsion angles about single bonds, although the extent of displacement of shifts could be varied in individual situations, e.g., variation of the torsion angle or functional groups attached. Previously, we found several kinds of conformation-dependent ^{13}C chemical shifts for the rotation about a single bond.[31-33]
In accordance with this expectation, we recently found that the CH_2O signals of the benzyl group are displaced by as much as 2.6 ppm, depending on amino acid composition as well as crystalline forms for a number of cyclic dipeptides containing L- or D-Glu(OBzl) group(s) (unpublished finding). Clearly, such significant displacement is caused by the presence of particular conformations defined by the χ_5 and χ_6 angles. Further, there appears a slight upfield displacement of the CH_2O signals (1.5 ppm) in going from the oligomers with $DP_n \leq 4$ to those with $DP_n \geq 5$, as indicated in Figure 1. Therefore, line broadening occurs when several conformers with various conformational angles are present, as in samples of lower crystallinity or amorphous materials.[31,32,34-36]
(31) Saitô, H.; Tabeta, R. *Chem. Lett.* **1981**, 713.
(32) Saitô, H.; Tabeta, R.; Hirano, S. *Chem. Lett.* **1981**, 1473.
(33) Saitô, H.; Izumi, G.; Mamizuka, T.; Suzuki, S.; Tabeta, R. *J. Chem. Soc., Chem. Commun.* **1982**, 1386.
(34) Schaefer, J.; Stejskal, E. O. *Top. Carbon-13 NMR Spectrosc.* **1979**, *3*, 283.
(35) Lyerla, J. R. *Contemp. Top. Polym. Sci.* **1979**, *3*, 143.
(36) Earl, W. L.; VanderHart, D. L. *Macromolecules* **1979**, *12*, 762.
(37) Recently, VanderHart et al. emphasized the importance of the anisotropic bulk susceptibility shift arising from aromatic rings for ^{13}C chemical shifts in the solid state when an aromatic moiety is present in samples.[38,39] Such effects also might contribute to the line broadening of the benzyl moiety when the side chains are disordered, although there appears no specific effect for the ^{13}C chemical shifts of the backbone carbons as manifested by observation of no sequence effect in the chemical shifts.
(38) VanderHart, D. L.; Earl, W. L.; Garroway, A. N. *J. Magn. Reson.* **1981**, *44*, 361.
(39) Earl, W. L.; VanderHart, D. L. *J. Magn. Reson.* **1982**, *48*, 35.
(40) Rothwell, W. P.; Waugh, J. S. *J. Chem. Phys.* **1981**, *74*, 2721.
(41) Hikichi, K. *J. Phys. Soc. Jpn.* **1964**, *19*, 2169.
(42) Miller, W. G.; Goebel, C. V. *Biochemistry* **1968**, *7*, 3925.
(43) Saitô, H.; Ohki, T.; Kodama, M.; Nagata, C. *Biopolymers* **1978**, *17*, 2587.
(44) Suzuki, Y.; Inoue, Y.; Chûjô, R. *Biopolymers* **1975**, *14*, 1223.
(45) Suzuki, Y.; Inoue, Y.; Chûjô, R. *Makromol. Chem.* **1980**, *181*, 165.
(46) The reported ^{13}C chemical shifts of the α-helix conformation of $[Glu(OBzl)]_n$ in 3% TFA/97% $CDCl_3$ are 56.3, 25.9, and 173.1 ppm for the C_α, C_β, and amide carbonyl carbons, respectively.[22]
(47) Sase, S.; Suzuki, Y.; Inoue, Y.; Chûjô, R. *Biopolymers* **1977**, *16*, 95.

Molecular Motion in Polycarbonates by Dipolar Rotational Spin-Echo ^{13}C NMR

Jacob Schaefer,* E. O. Stejskal, and R. A. McKay

Monsanto Company, Physical Sciences Center, St. Louis, Missouri 63167

W. Thomas Dixon†

Washington University, Department of Chemistry, St. Louis, Missouri 63130.
Received September 9, 1983

ABSTRACT: Molecular motions in polycarbonates and polycarbonate-like materials have been characterized by dipolar rotational spin-echo ^{13}C NMR. The dominant motion in polycarbonate is 180° flips about the aromatic-ring C_2 axes. These flips occur over a broad range of frequencies extending to over 15 MHz. The flips are superimposed on 30° ring oscillations about the same axes. Other main-chain motions, as measured through methyl-carbon dipolar patterns, are also significant; amplitudes of these motions are of the order of 20°. Chlorine substitution on the rings abolishes both ring and main-chain motions. Chemical modification of the links between rings also reduces motion, in some cases by preventing a fraction of the rings from flipping.

Introduction

The frequency of some of the main-chain motions of various polycarbonates has been determined from ^{13}C spin–lattice relaxation measurements employing high-resolution techniques, including magic-angle spinning.[1] In addition, the cooperative nature of main-chain motions has been inferred from the mechanical loss spectroscopy of an extended series of chemically substituted and modified polycarbonates and polycarbonate-like materials.[2] Despite the insights gained from such studies, to make an unambiguous connection between the macroscopic mechanical properties of these polymers and the microscopic molecular motions from which such properties derive, the amplitudes of the various ring and main-chain motions must be specified.

In this paper we measure the dipolar coupling between carbons and directly attached protons in polycarbonates using dipolar rotational spin-echo ^{13}C NMR.[3] The reduction in dipolar coupling by molecular motion (of frequency comparable to or greater than the dipolar coupling of about 10 kHz) becomes a measure of the amplitude of the molecular motion. Because this experiment is performed at natural abundance, it is practical to make such measurements on a series of polycarbonates, thereby aiding

† Present address: Washington University Medical School, Mallinckrodt Institute of Radiology, St. Louis, MO 63110.

0024-9297/84/2217-1479$01.50/0

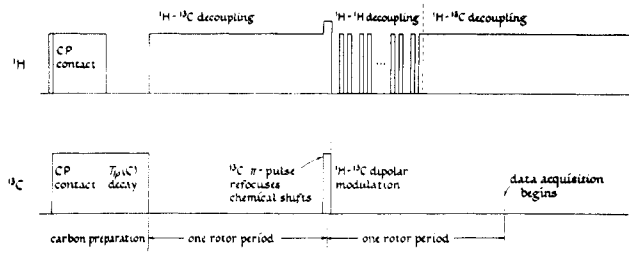

Figure 1. Pulse sequence for a dipolar rotational spin-echo ^{13}C NMR experiment. Following convention, ^{1}H–^{13}C dipolar modulation occurs in the time t_1, data acquisition in t_2, and $T_{1\rho}$(C) decay in t_3.

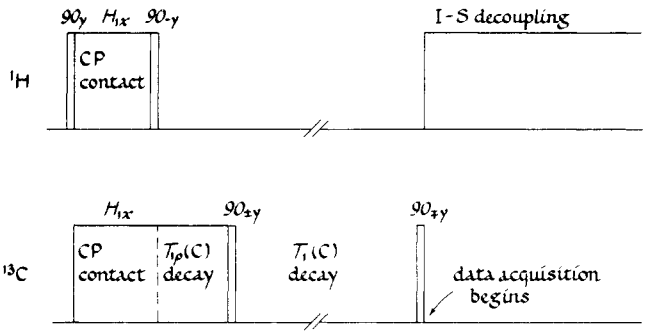

Figure 2. Pulse sequence for a double-select $T_{1\rho}$(C) and T_1(C) experiment.

in the assessment of the physical plausibility of our interpretation of motion.

Experiments

The pulse sequence for the dipolar rotational spin-echo experiment is shown in Figure 1. The evolution of the carbon magnetization due to chemical shift effects is refocused after two rotor periods by a carbon 180° pulse applied after the first rotor period. the ^{1}H–^{13}C dipolar modulation[4,5] is followed by varying the number of phase-shifted multiple-pulse ^{1}H (WAHUHA) pulse sequences[6] during a time t_1. The spinning speed is chosen so that an integral number of WAHUHA cycles exactly fits into one rotor period. In our experiments, this number was 16. Each WAHUHA cycle took 33 μs, with 3-μs 100° pulses,[7] so that sample spinning was at 1894 Hz. Experiments to characterize the weaker dipolar coupling for methyl carbons were sometimes performed at half the spinning speed using 32 WAHUHA cycles. Matched spin-lock transfers were performed at 60 kHz. Data acquisition took place during the time t_2. The time t_3 occurred in the preparation part of the sequence during which the carbons were spin-locked in the absence of a decoupling field. The pulse sequence of Figure 1 is similar to that used by Munowitz et al.[8] and by Munowitz and Griffin[9] for studying dipolar coupling in rotating solids.

Rotational dipolar sideband patterns were simulated by evaluating numerically integrals given by Herzfeld and Berger.[10] The double integral over α and β (eq 24 in ref 10) was performed by evaluating the integrand at 377 points on the unit sphere.[11] The integrand in the single integration over θ (eq 33 in ref 10) was evaluated at $\mu + 12$ points, where μ defines[10] the width of the dipolar pattern. Results of these calculations were tested by comparisons to published values.[10] Motionally modified dipolar and chemical shift anisotropy patterns were calculated by using the Herzfeld and Berger analysis, with width and asymmetry parameters evaluated from geometrical considerations under the assumption of fast motion (see Appendix).

The pulse sequence for a combined spin–lattice relaxation experiment is shown in Figure 2. This is a modified Torchia T_1(C) experiment in which carbon magnetization is generated by cross polarization, held spin-locked in the absence of a decoupling field for a variable time, and then restored to the z-axis direction by a 90° pulse.[12] Following waiting periods comparable to T_1 of the carbons, the surviving magnetization is sampled by a second 90° pulse. Phase cycling and data routing are employed to ensure inversion–recovery behavior.[12] With both T_1(C) and $T_{1\rho}$(C) delays

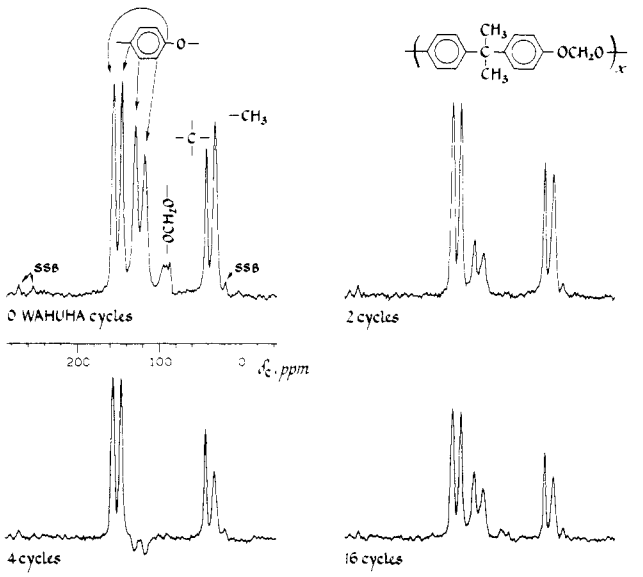

Figure 3. Dipolar rotational spin-echo 15.1-MHz ^{13}C NMR spectra of poly(BPA-formal) at room temperature as a function of the number of WAHUHA cycles used during ^{1}H–^{13}C dipolar evolution.

in the same experiment, it is possible, for example, to measure the megahertz-regime relaxation properties of a fraction of the sites of a dynamically heterogeneous material, with selection of those sites based on their kilohertz-regime behavior.

Relaxation measurements were made on a spectrometer built around a 12-in. iron magnet operating at a proton frequency of 60 MHz. Half-gram samples were spun with a single-bearing Beams–Andrew[13] type rotor. Some ^{13}C NMR spectra were obtained on a spectrometer built around a 3-in.-diameter bore superconducting solenoid operating at a proton frequency of 200 MHz. These spectra were used primarily for characterizing chemical shift anisotropies and were obtained with a double-bearing cylindrical rotor[14] capable of accurately controlled spinning speeds (±1 Hz) at 3 kHz.

The norbornylpolycarbonate used in these experiments was the kind gift of Dr. D. J. Massa (Eastman Kodak Co.), while the tetrachloropolycarbonate, poly(BPA-formal), and chloral polycarbonate materials were generously supplied by Dr. E. A. Williams (General Electric Co.). Polycarbonate itself is available commercially. All polymer samples for NMR analysis were prepared by slow cooling from the melt. Poly(BPA-formal) samples were prepared by both slow and rapid cooling from the melt. The latter two samples were made after several precipitations of the polymer from chloroform to remove low molecular weight impurities.

Results

Some chemical shift spectra (Fourier transforms with respect to t_2) as a function of WAHUHA irradiation during t_1 for annealed poly(BPA-formal) are shown in Figure 3. Protonated carbon magnetizations rapidly dephase under as little as 2 cycles of WAHUHA irradiation but are refocused after 16 cycles (one rotor period). Magic-angle spinning should refocus dipolar coupling just as it does chemical shift anisotropy, so in principle, an echo refocused following one rotor period of dipolar coupling should have the same intensity as one without any dipolar coupling. In fact, the former echo is only a third to a half as large. The losses are due primarily to incomplete ^{1}H–^{1}H decoupling. This source of error discriminates against protonated carbons (relative to nonprotonated carbons) but not against particular spatial orientations of C–H internuclear vectors.[3]

The centers of various lines in the spin-echo spectra were then Fourier transformed with respect to the dipolar evolution time, t_1. This was a 16-point Fourier transform

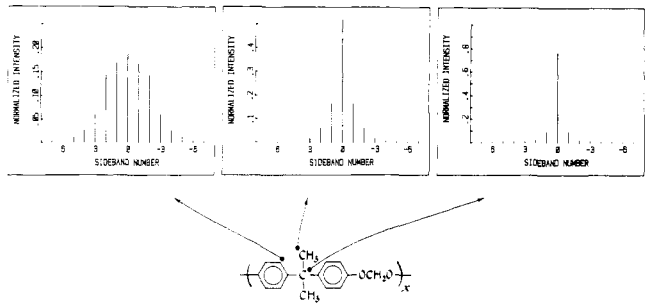

Figure 4. Dipolar Pake patterns for three carbons of poly(BPA-formal). Each pattern is broken up into spinning sidebands separated by 1.894 kHz. Each spinning sideband is represented by a single point in the frequency domain. The relative intensities of the displayed sidebands are representative of the true intensities, if we make the reasonable assumption of equal widths of sidebands.

Table I
Calculated Dipolar Rotational Sideband Intensities for an Aromatic CH Pair Undergoing Molecular Motion and Magic-Angle Spinning at 1894 Hz

motional model	sideband no. 0	1	2	3	4	5
static[a]	0.120	0.124	0.185	0.075	0.038	0.013
180° flips[b]	0.217	0.235	0.111	0.036	0.008	0.002
90° flips[c]	0.302	0.237	0.086	0.022	0.004	0.001
15° (rms) isotropic motion[d] plus 180° flips	0.269	0.239	0.095	0.026	0.005	0.001
9° (rms) isotropic motion plus 14° (rms) C_2 rolls plus 180° flips	0.298	0.237	0.087	0.022	0.004	0.001

[a] From Figure 5, top left. [b] From Figure 5, top right. [c] C_2-axis toggling between two positions separated by 90°. [d] Isotropic excursions from an equilibrium position with 15° rms amplitude.

resulting in a 16-point dipolar frequency spectrum. Examples are shown in Figure 4. Dipolar line shapes are broken up into sidebands separated by the spinning frequency of 1.894 kHz. Broad dipolar sideband patterns appear for carbons with strong CH coupling, with narrower patterns observed for carbons with weaker coupling such as that for the quaternary carbon of the isopropylidene unit. Over 80% of the intensity of the dipolar pattern for this carbon appears in the center band.

Large-amplitude motion about the ring symmetry C_2 axis can have a dramatic effect on the shape of the CH dipolar pattern (Figure 5 and Table I). The experimental aromatic-carbon dipolar patterns for most of the polycarbonates appear to be averaged by molecular motion. The patterns for norbornylpolycarbonate and polycarbonate, for example, are clearly narrower than that for the rigid crystalline BPA monomer (Figure 6). Because the second spinning sideband is near the maximum of a rigid dipolar Pake pattern under the conditions of our experiments, the ratio of intensities of the second to first dipolar rotational sidebands is a sensitive measure of averaging of CH dipolar coupling by molecular motion. This ratio changes from about 1.5 for systems with little motion to 0.5 for systems with substantial motion (Table II).

The aromatic CH n_2/n_1 dipolar sideband ratio also changes for some of the polymers as a function of the spin-lock delay time, t_3 (Figure 1). Carbons with substantial molecular motion near the rotating-frame Larmor frequency will have a short $T_{1\rho}$(C) relaxation time and escape the spin lock. The CH dipolar coupling pattern of the remaining carbon magnetization will therefore characterize the less mobile sites. For all the polymers of these experiments, about half the spin-locked carbon magnetization disappeared in 20 ms at 60 kHz in the absence of proton decoupling. But only the dipolar pattern of poly(BPA-formal) changes significantly (Table III); that of norbornylpolycarbonate has a weak dependence on the spin-lock delay time, while those of polycarbonate and chloral polycarbonate show no dependence (Table IV).

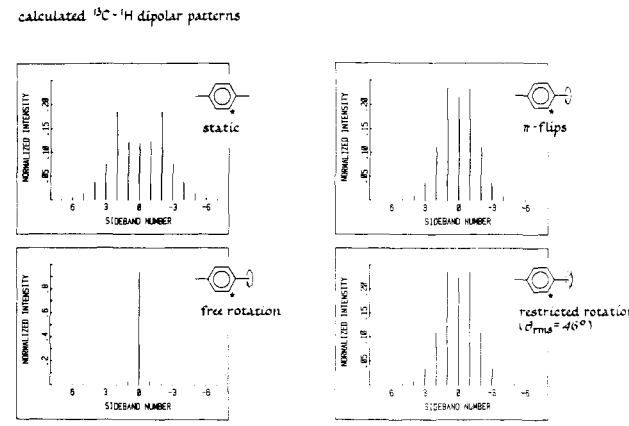

Figure 5. Calculated dipolar patterns for an aromatic CH pair under magic-angle spinning at 1.894 kHz, based on four different assumptions about molecular motion.

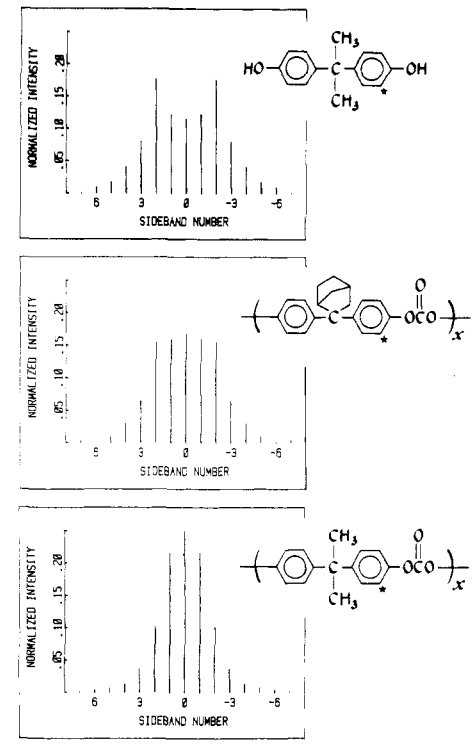

Figure 6. Experimental dipolar patterns for an aromatic CH pair under magic-angle spinning at 1.894 kHz for BPA monomer (top), norbornylpolycarbonate (middle), and polycarbonate (bottom).

Both the $T_{1\rho}$(C) and T_1(C) of polycarbonate have a weaker than square-law dependence on applied field (Table V), indicating the presence of a broad distribution of frequencies of motion. The $T_{1\rho}$(C) for polycarbonate has already been established[1,15] as a motional parameter over the entire range of H_1(C)'s reported in Table V. In addition, those sites in polycarbonate with longer $T_{1\rho}$(C)'s have shorter T_1(C)'s (Table VI). This behavior is opposite to that observed for polystyrene.[16]

The dipolar coupling tensor in a methyl group is more complicated than in an isolated CH pair. In one-fourth of the methyl groups the protons are either all spin up or all spin down. This triples the dipolar coupling seen by the carbon, but the threefold motion at an angle of 109°

Table II
Ratio of Intensities of Second to First Dipolar Rotational Sidebands

system	structure	n_2/n_1 protonated aromatic carbon (MAS = 1894 Hz)	n_2/n_1 methyl carbon (MAS = 947 Hz)
BPA (crystalline)	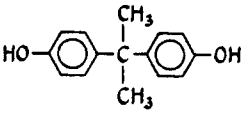	1.45	0.70
tetrachloropolycarbonate	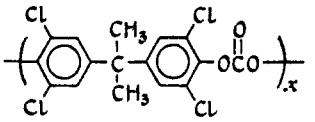	1.52	0.72
norbornylpolycarbonate	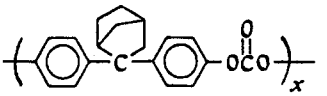	0.97	
poly(BPA-(formal)[a]	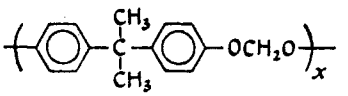	0.75	0.52
chloral polycarbonate	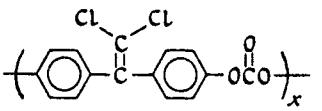	0.62	
polycarbonate	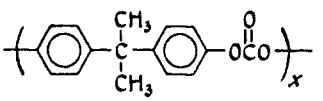	0.47	0.57

[a] Annealed material.

Table III
Experimental Dipolar Rotational Sideband Intensities for Polycarbonate and Poly(BPA-formal)

polymer	carbon	MAS freq, Hz	60-kHz spin-lock delay, ms	sideband no. 0	1	2	3	4	5
polycarbonate	CH	1894	0.05[a]	0.247	0.214	0.101	0.037	0.013	0.007
			20	0.263	0.218	0.096	0.037	0.013	0.003
	CH_3	947	0.05[b]	0.273	0.182	0.101	0.043	0.023	0.012
			20	0.273	0.176	0.104	0.039	0.031	0.006
poly(BPA-formal)[c]	CH	1894	0.05	0.242	0.200	0.102	0.036	0.021	0.009
			20	0.151	0.162	0.123	0.065	0.034	0.030
	CH_3	947	0.05	0.191	0.183	0.097	0.059	0.030	0.013
			20	0.264	0.181	0.094	0.049	0.026	0.017

[a] Dipolar pattern shown in Figure 6 (bottom). [b] Dipolar pattern shown in Figure 7 (bottom, right). [c] Quenched material.

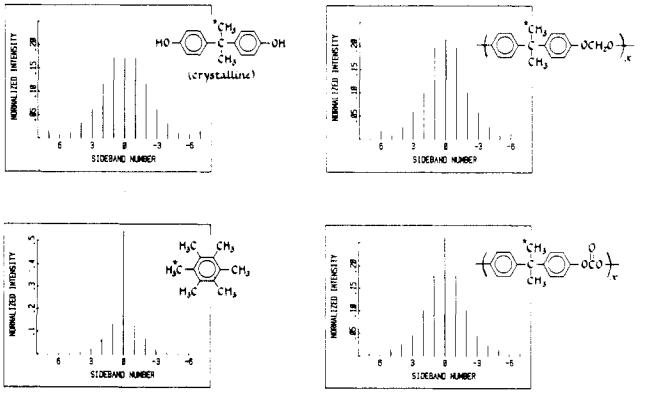

Figure 7. Experimental dipolar patterns for a methyl carbon under magic-angle spinning at 947 Hz for BPA monomer (top, left), annealed poly(BPA-formal) (top, right), polycarbonate (bottom, right), and hexamethylbenzene (bottom, left).

for the symmetry axis reduces the width of the dipolar tensor by a factor of 3. Therefore, these methyl groups have the same dipolar coupling as an ordinary CH pair. The other three-fourths have a tensor only one-third as strong because one proton spin opposes the other two. The

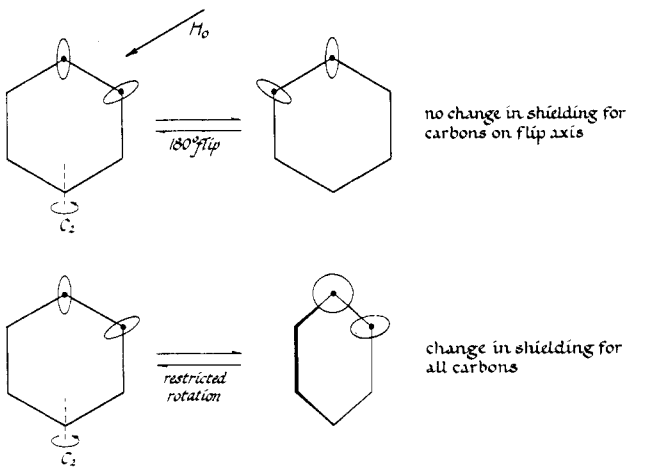

Figure 8. Schematic drawing showing the behavior of both on- and off-axis aromatic-carbon chemical shift anisotropies under 180° flips (top) and restricted rotational oscillations (bottom) about the ring C_2 axis. The 180° flip leaves the shielding to H_0 of the on-axis carbon unchanged regardless of orientation in the powder.

Table IV
Ratio of Intensities of Second to First Aromatic CH Dipolar Rotational Sidebands with MAS = 1894 Hz

^{13}C rotating frame spin-lock,[a] ms	n_2/n_1 poly-carbonate	poly (BPA-formal)[b]	chloral poly-carbonate	norbornylpoly-carbonate
0.05	0.47	0.75	0.62	0.97
3.00	0.44	0.87	0.64	0.97
8.00	0.47	0.95	0.61	1.05
16.00	0.44	1.06	0.61	1.06
20.00	0.45	1.28	0.62	1.10

[a] The pulse sequence of Figure 1 was used with t_3 varied. [b] Annealed material.

Table V
Field Dependence of Spin-Lattice Relaxation Times for the Protonated Aromatic Carbon of Polycarbonate

$H_1(C)$, kHz	$\langle T_{1\rho}(C)\rangle$,[a] ms	$H_0(C)$, MHz	$\langle T_1(C)\rangle$,[b] ms
20	5.2	15	107
28	6.6	50	370
37	7.4		
44	8.2		
60	8.6		

[a] Straight-line fit to the observed decay between 0.05 and 1.00 ms after the turnoff of $H_1(H)$. [b] Straight-line fit to the observed decay between 0.5 and 50 ms after z-axis restoration.

Table VI
Spin-Lattice Relaxation Times for the Protonated Aromatic Carbon of Polycarbonate in a Double-Select Measurement[a]

$T_1(C)$ delay,[b] ms	$\langle T_{1\rho}(C)\rangle$,[c] ms	$T_{1\rho}(C)$ delay,[d] ms	$\langle T_1(C)\rangle$,[e] ms
0.5	7.9	0.2	107
50	6.2	5	96

[a] The pulse sequence of Figure 2 was used with a 2-ms matched spin-lock contact at 44 kHz. [b] 37% of the signal has relaxed in 50 ms at 15 MHz. [c] Straight-line fit to the observed decay between 0.05 and 1.00 ms after the turnoff of $H_1(H)$ with $H_1(C)$ = 44 kHz. [d] 41% of the signal has relaxed in 5 ms at 44 kHz. [e] Straight-line fit to the observed decay between 0.5 and 50 ms after z-axis restoration.

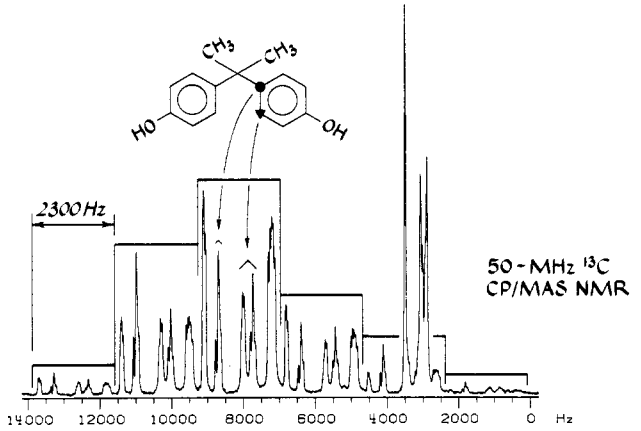

Figure 9. 50.3-MHz ^{13}C cross-polarization NMR spectrum of crystalline BPA with magic-angle spinning at 2300 Hz. The complexity of the spectrum arises from the presence of three molecules in the crystallographic unit cell. Each box in the spectrum outlines the aromatic-carbon peaks from spinning sidebands of a specific order. The grouping centered about 8000 Hz from (arbitrary) zero contains aromatic peaks at isotropic shift positions. The quaternary-carbon and methyl-carbon resonances are at 3500 and 3000 Hz, respectively.

Table VII
Calculated Dipolar Rotational Sideband Intensities for a Methyl-Group Undergoing Molecular Motion and Magic-Angle Spinning at 947 Hz

motional model[a]	sideband no. 0	1	2	3	4	5
static	0.172	0.183	0.110	0.042	0.035	0.017
15° (rms) isotropic motion[b]	0.209	0.190	0.099	0.041	0.030	0.013
30° (rms) isotropic motion	0.377	0.180	0.064	0.031	0.019	0.011
hexamethylbenzene-like motion	0.509	0.141	0.069	0.021	0.010	0.003

[a] With high-speed C_3-axis rotation assumed in all cases. [b] Isotropic excursions from an equilibrium position with 15° rms amplitude.

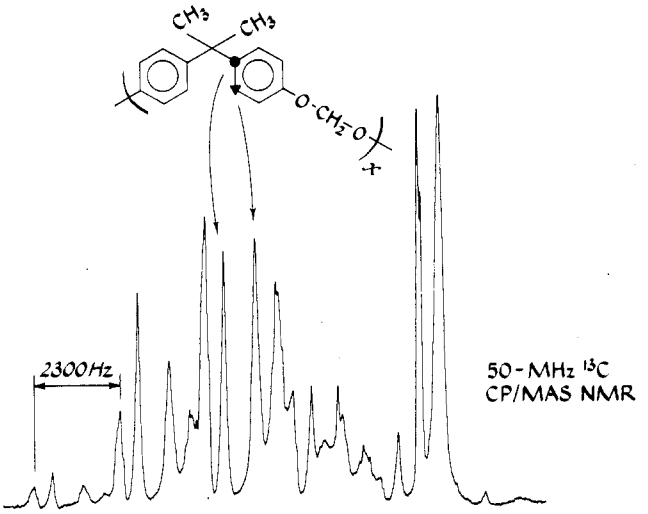

Figure 10. 50.3-MHz ^{13}C cross-polarization NMR spectrum of annealed poly(BPA-formal) with magic-angle spinning at 2300 Hz. The peaks arising exclusively from the carbons adjacent and ortho to the isopropylidene moiety are indicated by the solid circle and triangle, respectively. The peaks immediately to the left of the former and to the right of the latter arise from carbons para and meta to the isopropylidene moiety, respectively. The same assignments apply to the BPA spectrum of Figure 9.

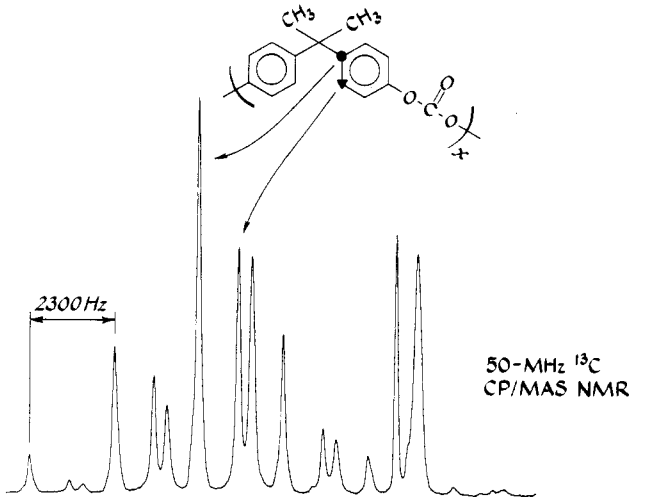

Figure 11. 50.3-MHz ^{13}C cross-polarization NMR spectrum of annealed polycarbonate with magic-angle spinning at 2300 Hz. The simplicity of this spectrum compared to that of BPA monomer in Figure 9 is due in part to averaging by molecular motion. The protonated aromatic carbon ortho to the isopropylidene moiety is indicated by the solid triangle. All nonprotonated aromatic carbons in polycarbonate contribute to the peak marked by the solid circle.

Table VIII
Chemical Shift Anisotropies at 50 MHz for Carbons Adjacent to the Isopropylidene Moiety of BPA (Monomer) and of Poly(BPA-formal) with Magic-Angle Spinning at 2300 Hz

	sideband no.				
system	2	1	0	−1	−2
BPA (monomer)					
obsd[a]	0.16	0.98	1.00	0.49	0.34
calcd[b]	0.20	0.98	1.00	0.49	0.34
poly(BPAformal)[c]					
obsd[d]	0.15	0.85	1.00	0.47	0.27
calcd[e]	0.15	0.82	1.00	0.46	0.28

[a] From Figure 9. [b] $\mu = 4.75$, $\rho = 0.50$. [c] Annealed material. [d] From Figure 10. [e] $\mu = 4.50$, $\rho = 0.43$.

weak methyl-carbon tensors are better studied at half the spinning speed used for the CH pairs. Figure 7 shows the dipolar sideband pattern for crystalline BPA monomer, poly(BPA-formal), polycarbonate, and hexamethylbenzene. The latter turns rapidly about the sixfold axis, producing additional averaging of dipolar coupling.[17] The dipolar patterns for the two polymers are intermediate in width relative to those of BPA and hexamethylbenzene. Some experimental second-to-first dipolar sideband intensity ratios for methyl carbons (at 947 Hz) are presented in Table II. For comparison, Table VII presents sideband patterns calculated for various motions.

Molecular motion can also modify the chemical shift tensor at various aromatic carbon positions (Figure 8). The 50-MHz ^{13}C NMR spectra of BPA monomer (Figure 9), poly(BPA-formal) (Figure 10), and polycarbonate (Figure 11) show pronounced sidebands with magic-angle spinning at 2300 Hz. The spectrum of BPA is complicated because there are three molecules in the crystallographic unit cell.[18] The spectrum of poly(BPA-formal) is especially informative because it has a separate peak for the ring carbons adjacent to the isopropylidene moiety (Figure 10, filled circle). In polycarbonate this resonance overlaps others. The reduced sideband intensities for both polymers relative to those for BPA show reduced chemical shift anisotropy tensors. It is unlikely that these differences are the result of chemical modification, at least for carbons near the isopropylidene moiety since those sites are well removed from the area modified on polymerization. Rather, such reductions appear to be due to molecular motion. Experimental values for the spinning sideband intensities for the carbons of BPA and poly(BPA-formal) adjacent to the isopropylidene moiety are presented in Table VIII.

Discussion

Dipolar Coupling and Large-Amplitude Motion. Since all CH bonds are about 1.085 Å long, it is motion that causes the variety of observed dipolar coupling tensors (Figure 6). In general, collapse of dipolar tensors is not a particularly sensitive method for detecting motions, but it is a method that allows one to say something about the size and type of large-amplitude motions. As we show below, these tensor studies are particularly well suited to the polycarbonate family because of the presence of such motions.

To get an immediate appreciation for the magnitude of typical polycarbonate motions, compare the simulated dipolar spinning band patterns of Figure 5. The top left pattern arises from a static CH pair. The lower left pattern arises from the ortho (or meta) CH pair in an aromatic ring freely rotating about the ring C_2 axis. The strength of the dipolar coupling tensor for the latter is reduced by a factor of 8 relative to the former, because the 60° angle between the CH axis and the spinning axis is close to the magic angle. The two patterns on the right, which are more like that of polycarbonate than either of the two on the left, represent large-amplitude hindered rotations about the C_2 axis.

A given motion results in a unique dipolar spinning sideband pattern but a given pattern does not specify a unique motion. The patterns at the right-hand side of Figure 5 result from either of two easily described large-amplitude hindered rotations. One motion is 180° flips about the C_2 axis. The ring spends exactly half its time on each side and none on edge—just like a fish in a frying pan. This motion has been proposed for phenylalanine[19] and tyrosine[20] rings in amino acid crystals. The same pattern (within a few percent) also results from a rolling motion about the C_2 axis. The rolling motion assumes all angular positions within ±65° of an equilibrium position are occupied equally but that angles greater than 65° from equilibrium are blocked out. We will discuss later a method for distinguishing which of these two motions occurs in polycarbonate.

The degree of collapse of the dipolar tensor generated by some individual large-amplitude hindered motions matches or exceeds the total narrowing observed experimentally, and so these motions can be ruled out immediately. This is the situation, for example, for 90° flips (i.e., toggling between two positions separated by 90°) about the C_2 ring axis for polycarbonates (Tables I and III). This motion by itself accounts for all the observed collapse of the aromatic CH dipolar tensor; its widespread presence in polycarbonate would preclude that of any other motion, an impossible situation (cf below). Free rotation (which is equivalent to toggling between four positions separated by 90°) can also be ruled out. While the observed dipolar patterns for polycarbonate still are consistent with many motional models, such as 180° flips or ±65° rolls, it is absolutely impossible for any small-amplitude motion to collapse the dipolar tensor so much. Our first firm conclusion then is that polycarbonate is right behind liquid crystals and rotor crystals in terms of amplitude of motion in the solid state. A second firm conclusion is that ordered by motion, polycarbonate > chloral polycarbonate > poly(BPA-formal) > norbornylpolycarbonate ≫ tetrachloropolycarbonate.

Amplitude Heterogeneity of Ring Motion in Polycarbonates. To see if ring motions throughout a glassy sample are all about the same amplitude, dipolar coupling can be measured after a long carbon spin lock in the absence of proton decoupling. During this spin lock, carbon spins lose magnetization according to their individual $T_{1\rho}$(C)'s. If there is more than one ring population, one with a long $T_{1\rho}$ and the other with a short $T_{1\rho}$, comparing results of this modified experiment with those from the ordinary experiment will show whether or not the long-$T_{1\rho}$ part of the sample has the same dipolar coupling as the short-$T_{1\rho}$ fraction. For poly(BPA-formal) a distinct difference between the two populations is seen for both quenched (Table III) and annealed (Table IV) samples.

After a 20-ms spin-lock hold, the aromatic CH dipolar pattern of the annealed poly(BPA-formal) looks a lot like that of crystalline BPA itself (see Figure 3 from ref 3) with an n_2/n_1 sideband ratio of 1.28 (Table IV). The quenched material behaves similarly although the difference caused by the spin-lock delay is not quite so dramatic. About half of the protonated aromatic-carbon magnetization of annealed poly(BPA-formal) disappears after a 20-ms carbon spin-lock at 60 kHz. We conclude that about half the rings in annealed poly(BPA-formal) can be considered mobile and have dipolar sideband patterns that look like that of polycarbonate (with $n_2/n_1 \sim 0.5$), and the other half are

immobile with dipolar patterns reflecting near static CH coupling. It is reasonable to suppose interchain packing is responsible for this motional heterogeneity because of the sensitivity to thermal history. A motional amplitude heterogeneity seems also to be present for norbornyl-polycarbonate, but not for chloral polycarbonate or for polycarbonate itself (Table IV). Only the polymers with lower average mobility show a motional amplitude heterogeneity.

Frequency Heterogeneity of Ring Motion in Polycarbonates. While we have no evidence the amplitude of ring motion in annealed polycarbonate is inhomogeneous, we know the frequency must be. This inhomogeneity can be read directly in the curvature of spin–lattice relaxation plots of protonated ring carbons in polycarbonate,[15] provided of course ring motion is the cause of the relaxation. This is, in fact, the situation since T_1(C) and $T_{1\rho}$(C) relaxation of the aromatic carbons is much faster than the corresponding methyl-carbon relaxation. Therefore, the curved T_1(C) and $T_{1\rho}$(C) plots typical of polycarbonate necessarily show inhomogeneity in the polymer. Different spins have different decay constants and if these differences cannot be attributed to inhomogeneous amplitudes of ring motions, then the motions must occur at different frequencies.

Frequency heterogeneity is also responsible for the lack of pronounced broadening of the protonated aromatic-carbon line of polycarbonate as the temperature is lowered.[21] Such broadening is observed, for example, for the methyl-carbon resonance of crystalline polypropylene, which disappears altogether at 133 K and then reappears at lower temperatures.[22] This broadening can be ascribed to interference by motion with resonant proton–carbon decoupling at about the same frequency.[23] For polycarbonate, however, only a fraction of the sample, at a given temperature, will ever have motion near the decoupling frequency and hence be susceptible to broadening.

Frequency heterogeneity is evident when we estimate the ring frequency for polycarbonate. We have two ways to make such an estimate and they lead to completely different numbers. The first is a comparison of T_1(C) at 15 and at 50 MHz. For the protonated aromatic carbons in polycarbonate the respective values are 107 and 370 ms (from the initial slopes, an average over the sample). If characteristic ring frequencies were below 15 MHz, the T_1 would vary with the square of frequency and the high-field T_1 would be about 10 times the low-field value. On the other hand, if characteristic frequencies were all greater than 50 MHz, the two T_1(C)'s would be about the same. Either the characteristic frequency is a little over 15 MHz or it is distributed, with some above and some below 15 MHz.

The other way to estimate the characteristic ring flip frequency relates the second moment of the CH dipolar coupling in polycarbonate to measured $T_{1\rho}$(C)'s. We know that $1/T_{1\rho}$(C) is determined by CH dipolar field fluctuations orthogonal to H_1(C).[24] We are concerned only with those fluctuations that are also in the same direction as H_0, since those orthogonal to H_0 give rise to $1/T_1$(C), and we know $1/T_1$(C) is much smaller than $1/T_{1\rho}$(C). Because static CH dipolar interactions depend only on coupling along H_0, fluctuations in local fields along H_0 also lead to the diminution in the polycarbonate CH second moment relative to its rigid lattice value. In other words, the same fast ring motion that gives rise to such short $T_{1\rho}$(C)'s in polycarbonate is also responsible for the reduction of its CH second moment.

We assume $1/T_{1\rho}(C) = c^2J(\omega) = c^2[1/(1 + \omega^2\tau_c^2)]$, where the strength of the coupling is given by c^2, the relevant spectral density by $J(\omega)$, and the characteristic ring frequency by $1/\tau_c$. We evaluate c^2 at $\omega = 0$ from the observed approximately ω-independent $T_{1\rho}$(C) of about 8 ms. Thus, $c^2 = (8\text{ ms})^{-1}$. The change in second moment, ΔM_2, between polycarbonate and a rigid lattice (modeled by, say, crystalline BPA[25]) can be identified approximately as the change in the square of a CH line width due to motion. This means ΔM_2 can be identified as the change in the squares of all CH local dipolar fields. These fields are just the interactions giving rise to $1/T_{1\rho}$(C). Hence $\Delta M_2 \cong 2\int_0^\infty c^2[1/(1 + \omega^2\tau_c^2)]\,d\omega = \pi c^2/\tau_c$ and $1/\tau_c \cong \Delta M_2/\pi c^2$. Taking second moments of dipolar spinning sideband patterns, one gets 58 and 25 $(\text{kHz})^2$ for rigid model materials and polycarbonate, respectively. Substituting values, we conclude that the characteristic ring frequency, $1/\tau_c$, is of the order of 300 kHz.

Comparing this result with the T_1(C) experiments defines the extent of the frequency heterogeneity. Characteristic ring frequencies in polycarbonate are spread from 300 kHz up to about 25 MHz. The H_1(C) dependencies of $T_{1\rho}$(C) (Table V) may require frequencies even less than 60 kHz, but at lower frequencies it is hard to be sure the C_2 ring motion which narrows the dipolar tensor also dominates $T_{1\rho}$(C) relaxation. Other smaller amplitude main-chain motions may be important to $T_{1\rho}$(C) (cf below). We suspect, but cannot prove at this point, that the frequency heterogeneity in polycarbonate is due to packing effects, just as packing is responsible for the motional amplitude heterogeneity in poly(BPA-formal).

One further manifestation of the frequency heterogeneity in polycarbonate is perhaps worth mentioning. Since there is no obvious amplitude variation from site to site in annealed polycarbonate at room temperature, those sites with rings undergoing fast large-amplitude megahertz motion should have short T_1(C)'s and long $T_{1\rho}$(C)'s, with the opposite expectation for those sites with rings undergoing slow large-amplitude kilohertz-regime motions. These expectations are indeed observed (Table VI).

Main-Chain Motion. The C_2-axis ring motions in polycarbonate do not drag the methyl groups along, but main-chain motions do. Methyl dipolar coupling can be examined to see if C_2-axis motions are the only motions with appreciable amplitude in polycarbonates.

Methyl dipolar spectra are not as easy to use as CH dipolar spectra. First, the average CH_3 dipolar couplings are weaker so slower spinning is required. This means taking more data points in the dipolar evolution dimension (32 WAHUHA cycles instead of 16), and the longer delay (still 2 rotor revolutions) before refocusing reduces the signal-to-noise ratio. Second, proton–proton coupling is tight, making WAHUHA decoupling more critical and so further reducing refocusing and signal to noise. Finally, the methyl spectrum is a superposition of spectra from the four different proton spin states in methyl groups. For a CH pair only two spectra are superposed, one for protons spin up and one for spin down. The extra spin states for methyl groups make it more difficult to fit parameters to the observed spectrum.

Despite the difficulties associated with methyl groups, methyl dipolar spectra (Figure 7 and Table II) clearly indicate increasing motion in the order BPA, poly(BPA-formal), polycarbonate, and hexamethylbenzene. This is not a surprising order. The first three are in the same order as seen for the protonated aromatic carbons, while hexamethylbenzene is known to undergo rapid large-amplitude motion about the ring sixfold axis.[17] For comparisons, Table VII presents simulated methyl spectra for

methyl groups with only C_3 motion, for methyl groups undergoing additional 15° and 30° root-mean-square isotropic angular motions (see the Appendix for a definition of the rotation axes), and for methyl groups with free rotation about an axis perpendicular to the threefold axis (as occurs in hexamethylbenzene). These methyl dipolar pattern simulations are based on sample spinning at half the rate used in the aromatic carbon experiments but assume the same scaling factor for the WAHUHA decoupling. The two polymer methyl-carbon dipolar patterns are reasonably well fit using a 15° (root mean square) isotropic motion model.[26] We conclude that methyl motions in polycarbonate and poly(BPA-formal) are smaller in amplitude than the motions of the aromatic rings of the two polymers but larger than either the ring or methyl motions in typical organic crystals like BPA. On the basis of comparisons of dipolar patterns, these methyl motions in polycarbonate have no apparent amplitude heterogeneity (Table III and are clamped by chlorine ring substitution (Table II).

Establishing Ring Flips by Chemical Shift Anisotropies. The collapsed protonated aromatic dipolar coupling tensors prove several of the polycarbonates examined have large-amplitude, rapid ring motions but, as discussed earlier, cannot show whether the rings are actually flipping all the way over. (See text associated with Figure 5.) Large-amplitude motions in the methyl group would have ruled out ring flips. The methyl motions necessarily require ring motions, and 180° flips superimposed on an already reduced dipolar coupling would have resulted in coupling smaller than that observed. However, the methyl motions in polycarbonate are not large-amplitude, and considering the uncertainty in the magnitude and direction of such motions, no firm conclusion about ring flips based on the methyl-carbon dipolar patterns can be drawn.

Experiments detecting collapsed ^{2}H NMR quadrupolar patterns have been used to argue for the presence of 180° flips in crystalline amino acids like phenylalanine.[19,21] The narrowed patterns have characteristic dual peaks or cusps ("rabbit ears") whose position and shape are almost temperature independent. The same sort of a line shape identification can be troublesome in glassy polymers, however, where dynamic heterogeneity is the norm rather than the exception. Thus, if all polymer sites have fast, reasonably large-amplitude motions, 10% acting as free rotors will produce characteristic "rabbit ears", whose position will be insensitive to temperature and not necessarily subject to discrimination by T_1 or $T_{1\rho}$-like selection techniques.[21] Depending on the clarity and resolution of the rest of the pattern, it may be impossible by ^{2}H NMR to establish the likely presence of 180° flips, as opposed to some other distributed rolling motion mixed in with some free rotors.

A natural place to look to solve this problem of the extent of ring flipping is to the chemical shift anisotropy of carbons directly on the ring C_2 axis. These carbons are not bound to a proton (or deuteron), so dipolar (or quadrupolar) coupling does not help here. Most importantly, 180° flips about the C_2 axis do not affect the chemical shift tensors of these carbons, but large rolling motions about that axis do (Figure 8). Rolling motions leave the high-frequency or low-field principal component which lies along the C_2 axis alone but average the other two principal components.

Unfortunately, resonances from carbons on the C_2 axes in polycarbonate overlap each other. But the carbons directly attached to the isopropylidene moiety in both BPA and poly(BPA-formal) are resolved (Figures 9 and 10). Reasonable fits to the 50-MHz ^{13}C NMR spectra of these carbons are obtained with CSA μ values of 4.75 and 4.50 for BPA and annealed poly(BPA-formal), respectively, and ρ values of 0.50 and 0.43, using the notation of Herzfeld and Berger[10] (Table VIII). In terms of principal components, these fits translate to 91, 36, and −127 for BPA and 89, 30 and −118 for the polymer, as expressed in parts per million from the isotropic peak. All three principal components change more on polymerization than does the isotropic peak and so are probably a measure of motion and not chemistry. The principal component least affected lies along the C_2 axis of the ring, confirming that motion is primarily about that axis. The BPA chemical shift tensor for the carbon adjacent to the isopropylidene unit can be turned into the corresponding polymer tensor by 9° (root mean square) isotropic motion superimposed on 14° (root mean square) motion about the C_2 axis (see Appendix). The BPA chemical shift tensor cannot be turned into the polymer tensor by large-amplitude rolling motions about the C_2 axis. Such motions produce changes in the tensor far larger than those observed. Thus, ±65° rotations are absolutely ruled out as an explanation of the observed aromatic CH dipolar patterns. Similar arguments can be used to eliminate C_2-axis 90° flips, as well as large-amplitude isotropic motions about an equilibrium point.

Dipolar patterns for the carbons ortho to the isopropylidene unit can be simulated assuming 9° (root mean square) isotropic and 14° (root mean square) rolling motions with (Table I) and without 180° flips. Examining only the n_2/n_1 dipolar sideband intensity ratio and assuming a WAHUHA scaling factor[3] to yield a static dipolar n_2/n_1 ratio of 1.50, the ratios are 0.37 and 1.18 with and without 180° flips, respectively. The observed values for quenched and annealed poly(BPA-formal) are 0.51 and 0.75, respectively. These observed values are inconsistent with either none or all of the rings flipping but allow some of the rings to flip while some do not. The same conclusion holds for chloral polycarbonate. With its larger and more homogeneous motion (and an n_2/n_1 dipolar ratio of 0.45), it seems reasonable to conclude that in polycarbonate itself most of the rings flip. For norbornylpolycarbonate (with a protonated aromatic carbon n_2/n_1 dipolar sideband ratio close to 1.0 (Table II)) few of the rings can flip, while for tetrachloropolycarbonate none of the rings flip.

The chemical shift anisotropy of the ortho or meta carbons may also be a place to look for the answer to the question of the extent of ring flipping in polycarbonate. Analysis of the chemical shift anisotropy can be informative even though the dipolar coupling tensor analysis for these carbons was ambiguous. This is true because in general the unaveraged CSA tensor has less symmetry. Also, the CSA spinning sideband pattern contains more information because it is not forced into left–right symmetry by an equal number of spin-up and spin-down protons, as is the situation for the dipolar coupling pattern. The difficulty in using the CSA to characterize motion is in obtaining experimental values for the motionally unaveraged tensor.

It is known that aromatic carbons with the CH bond along the field resonate at the highest frequency, and those with rings perpendicular at the lowest.[28] Flips do not affect the lowest frequency but partially average the two higher frequency principal components together. Examining the Herzfeld and Berger tables,[10] one sees that the primary effect of this averaging is to decrease the first lower frequency spinning sideband relative to the isotropic peak

(provided $\mu < 12$). The first higher frequency sideband may increase or decrease, depending upon μ.

Rolling motions about the C_2 axis have the *opposite* effect. Since the sideband of order 1 of the carbon ortho to the isopropylidene unit is initially larger than that of order −1 for BPA monomer, rolling motions in the polymer will make both sidebands tend toward the same size or might even make the n_{-1} sideband greater than the n_1 sideband. Comparison of Figures 9 and 11 shows that the n_{-1} sideband (the high-field first spinning sideband) is reduced relative to the center band more than the n_1 sideband when BPA is polymerized. Thus, from this qualitative trend of spinning sideband intensities alone, we can conclude that the rings in polycarbonate are flipping all the way over, rather than undergoing large-amplitude rolls.

Summary of Conclusions for Motion in Polycarbonate. We summarize the results for motion in annealed polycarbonate in this section. Polycarbonate motion at room temperature has amplitude homogeneity throughout the glass but frequency heterogeneity, with many of the frequencies greater than 300 kHz. The rings undergo 180° flips (not ±65° rolling motion) as established from the chemical shift anisotropies of both on- and off-C_2 axis carbons. The resulting predicted dipolar sideband pattern for protonated aromatic ring carbons undergoing 180° flips shows insufficient collapse (Figure 5, top right, and Figure 6, bottom); there must be additional motion. The isopropylidene methyl-carbon dipolar pattern is consistent with a 15° (root mean square) isotropic main-chain motion (Table VII and Figure 7). This motion added to the 180° flips for the rings would yield an aromatic dipolar pattern close to that observed (Tables I and III). However, such a main-chain motion seems physically implausible. A good fit to the observed chemical shift anisotropies of the ring carbons is achieved with a 9° (root mean square) isotropic motion mixed with a 14° (root mean square) C_2 rolling motion (Table VIII and Appendix). This combination can be thought of as approximating a physically plausible, cooperative, anisotropic main-chain motion. Such a motion in concert with 180° flips then results in a model that predicts reasonable (not perfect) fits to experiment for ring-carbon chemical shift anisotropies, ring-carbon dipolar patterns, and methyl-carbon dipolar patterns. A 9° (root mean square) isotropic excursion translates into a 20–25° total angular main-chain displacement, while a 14° (root mean square) rolling motion means a total azimuthal angular displacement about the ring C_2 axis of about 30–40°.

These conclusions are in agreement with the results of ^{1}H, ^{2}H, and ^{13}C NMR experiments on specifically labeled polycarbonates. The ^{2}H NMR of polycarbonate deuterated only in the ring reveals a line shape[29] consistent with extensive 180° flips together with smaller angle rotations about the ring C_2 axis. Furthermore, polycarbonate synthesized with the methyl protons replaced by deuterons has a low-temperature ^{2}H NMR spectrum about 10% narrower than expected for C_3 rotation alone,[30] one explanation for which is the presence of an additional high-frequency motion affecting the methyl group. (Spiess, however, feels this conclusion is not justified.[29,30]) Next, the ^{1}H NMR of methyl-deuterated polycarbonate has a line shape showing only minor narrowing due to motion.[31] This is to be expected if the dominant ring motion present is 180° flips about the C_2 axis since that motion leaves unchanged the dipolar coupling between C_2 and C_6 protons. (No motion about the C_2 axis affects coupling between C_2 and C_3 protons.) Finally, analysis of the ^{13}C chemical shift anisotropy of a nonspinning polycarbonate, ^{13}C enriched ortho to the carbonate moiety, also suggests the presence of 180° flips superimposed on smaller rotational oscillations about the C_2 axis.[32]

Reliability of Interpretations of Dipolar Patterns. A detailed description of motion in polycarbonate was presented in the previous section. It is reasonable to ask about the reliability of such an assignment, particularly in view of the extensive use of the results of the dipolar modulation experiment, a new analytical technique.

To increase the confidence one can place in the interpretation of dipolar modulation experiments, we have chosen to interpret only differences in dipolar patterns. That is, we attach significance only to trends within a family of dipolar couplings, such as those shown in Table II. Even in comparing motionally averaged dipolar patterns with those expected from a rigid lattice, we use results from an experimental rigid crystalline system. There are no comparisons to absolutes.

Next, we base out motional models not just on dipolar couplings, but on these couplings together with information from chemical shift anisotropies, T_1(C)'s and $T_{1\rho}$(C)'s. For example, we have made clear that the observed aromatic-carbon dipolar sideband pattern for polycarbonate is consistent with 180° flips plus an additional minor motion. The additional motion could be any one of a variety of forms: isotropic motion within a small sector, C_2-axis rotations, or some combination of these. Results from the CH dipolar modulation experiment cannot distinguish between these possibilities. However, by combining aromatic CH dipolar coupling information with that for methyl-carbon dipolar coupling and with information from aromatic carbon chemical shift anisotropies, a reasonable choice can be made. Even though we arrive at a detailed model for the motion, we feel we have not overinterpreted the results of any single experiment.

Finally, we recognize that in dealing with glassy polymers like polycarbonate, we are faced with a heterogeneous system. The possibility exists of distortions in CH dipolar line shapes arising from powder orientation effects, from $T_{1\rho}$(C) heterogeneity, and from molecular motion at frequencies comparable to sample spinning rates, WAHUHA cycle rates, or CH decoupling frequencies. In part, our strategy of interpreting only differences in dipolar patterns was formulated because of complications that can arise from sample heterogeneity. Thus, if powder orientation poses a problem, we should see the effects of this problem in the sideband pattern for crystalline BPA (compare Figures 5 and 6). Or, if $T_{1\rho}$(C) heterogeneity can distort dipolar patterns, then using $T_{1\rho}$(C) delays as part of the carbon-magnetization preparation (Figure 1) should reveal the complication. The fact that polycarbonate CH dipolar patterns are totally insensitive to such delays, while those for poly(BPA-formal) are not (Table IV), convinces us that $T_{1\rho}$ distortions are not serious and that we can interpret the trends observed for poly(BPA-formal).

Naturally, all of our measurements are sensitive to interference from molecular motion at unfortuitous frequencies. Some line broadening in the dipolar-decoupled spectra of polycarbonate is known to arise from the presence of molecular motion in the mid-kilohertz frequency regime,[1] the same frequency as the radio-frequency decoupling field. But this is not a major effect; and its presence does not prohibit our observing and using ^{13}C NMR spectra of polycarbonate in the solid state. In fact, it is the pronounced heterogeneity of frequency of motion in polycarbonate-like systems that saves us here. Motion is not concentrated at any single frequency, so distortions

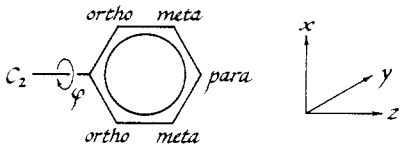

Figure 12. Coordinate axes to describe ring motion.

from interferences are necessarily minor. For example, we expect interferences of this type with refocusing of a dipolar echo can amount to no more than a few percent. None of our conclusions depend on differences in dipolar sideband patterns of this magnitude.

Connection between Molecular Motion in Polycarbonates and Mechanical Properties. This section can be brief and will include a list of results still needed to make an unambiguous connection between microscopic motion in polycarbonates and macroscopic properties. From dipolar patterns we have established the presence of a main-chain motion coupling polycarbonate rings with the isopropylidene unit. The motion has amplitude homogeneity in the glass and is clamped by ring substitution. The motion operates above 60 kHz at room temperature, and probably above 300 kHz, and is necessarily mechanically active. The latter two conclusions derive from the weak H_1(C) dependence of both methyl- and aromatic-carbon $T_{1\rho}$'s observed for polycarbonate[1,15] and from general interpretations of the mechanical loss behavior of polycarbonates by Yee and Smith.[2]

We have also established the presence of extensive 180° flips in several polycarbonates. This motion is a restricted rotation. Calculations of conformational populations for an isolated single polycarbonate chain show that rotation about the ring C_2 axis should be virtually free[33] but that the motions of the two rings in the BPA unit are correlated. The change from a free rotation to a restricted rotation for both rings of the repeat unit is the result of constraints placed on one or both of these rings by adjacent chains and, in particular, by the rings of adjacent chains that form the glassy lattice. Flipping of a ring therefore demands some distortion of the lattice, a process which is itself mechanically active.

The observed frequency heterogeneity for ring flipping in polycarbonate matches the position and breadth of the γ transition of typical tan δ mechanical loss spectra,[2] at least hinting at a connection. It is not clear from our results, however, the *degree* to which the 180° flips are coupled to main-chain motion and to each other. That is, we do not know from ^{13}C NMR results alone whether *all* the ring flips are part of the same cooperative motion and hence equally mechanically lossy. Yee and Smith[2] have concluded that ring flips may be present in polycarbonates but are *not* involved in the γ transition. Experiments employing multiple-quantum NMR[34] of specifically deuterated polycarbonates are in progress and are designed to approach the question of the cooperativity of ring motion directly.

Finally, before mechanical properties such as stress–strain behavior can be inferred from descriptions of microscopic motions, we need some sort of a definition of the role of glassy-state packing in polycarbonate. In particular, we need to specify how packing can create a heterogeneity in frequency but not in amplitude of motion. The answer to this question is probably linked to polycarbonate rings undergoing 180° flips rather than, say, correlated 90° flips, as might be expected from symmetry arguments for isolated chains.[33] Such questions about packing may yield to analysis employing computer modeling of glasses.

Acknowledgment. This work was supported in part by Grant DMR-8007025 from the Polymer Division of the National Science Foundation.

Appendix

This section gives useful formulas and results for simple cases of motionally averaged tensors, particularly tensors for phenyl rings moving about their C_2 axes.

Notation and Calculations. For convenience we express tensors with principal components assigned in order of frequency, $\omega_{33} \geq \omega_{22} \geq \omega_{11}$. The origin of the frequency axis is chosen so that $\omega_{33} + \omega_{22} + \omega_{11} = 0$. All calculations are based on the equation $\omega = \langle\lambda_3^2\rangle\omega_{33} + \langle\lambda_2^2\rangle\omega_{22} + \langle\lambda_1^2\rangle\omega_{11}$, where the λ's are the cosines of the angles between the magnetic field and the principal axes of the instantaneous, unaveraged tensor. The brackets indicate a time average over the motion. Axes for the phenyl-ring equilibrium positions are shown in Figure 12, with the z axis selected along the ring C_2 axis and the y axis perpendicular to the ring.

The three principal components of a tensor are easily seen in a static powder pattern. They are the maximum and minimum frequencies and the frequency at the cusp. Although none of these components is easily determined by simple inspection of a spinning sideband pattern, the symmetry of the tensor can be determined. If the largest spinning sideband is on the high-frequency side of the isotropic peak, then the intermediate principal component lies closer to the highest frequency component than to the lowest, and vice versa.

To determine the three principal components from a spinning sideband pattern, Herzfeld and Berger's[10] technique is used. To switch between their μ,ρ notation and principal components, we use the following formulas: $\mu = \omega_{33} - \omega_{11}$ and $\rho\mu = 3\omega_{22}$, with $\omega_{33} = (1 - \rho/3)\mu/2$, $\omega_{22} = \rho\mu/3$, and $\omega_{11} = -(1 + \rho/3)\mu/2$.

Axially Symmetric CH Dipolar and ^{2}H Quadrupolar Tensors. Since protons in a sample are just as likely to be spin up as spin down, both static and spinning spectra affected by axially symmetric tensors are mirror symmetric. For convenience we scale the unaveraged tensor components for half the spins to 1, $-^1/_2$, and $-^1/_2$ with the other half at $^1/_2$, $^1/_2$, and -1.

For isotropic excursions from equilibrium, the tensor symmetry is not affected, but the principal components shrink. Along the principal axis $\omega_{33} = \langle\cos^2\theta\rangle(1) + \langle\cos^2(\pi/2 - \theta)\rangle(-^1/_2) + \langle\cos^2(\pi/2)\rangle(-^1/_2)$. This simplifies to $\omega_{33} = 1 - 3\langle\sin^2\theta\rangle/2$, where θ is the deviation from equilibrium position. The other new components are both $-\omega_{33}/2$.

For phenyl-ring motion about the C_2 axis, only the ortho and meta positions need consideration; the on-axis sites with axially symmetric tensors are unaffected by C_2 motions. We will consider four examples of this kind of motion. (1) For 180° flips, the principal component perpendicular to the ring is unchanged by the motion, but the x and z axes are now symmetry axes so that $\omega_{xx} = ^5/_8$, $\omega_{zz} = -^1/_8$, and $\omega_{yy} = -^1/_2$. (2) For free rotors, the new tensor is symmetric about the C_2 axis with $\omega_{zz} = -^1/_8$ and $\omega_{xx} = \omega_{yy} = ^1/_{16}$. It is worth noting that both 180° flips and free rotors have a component near zero. This leads to prominent cusps or "rabbit ears" in the center of the powder pattern. If 180° flips are present, the position of these rabbit ears is relatively insensitive to additional rolling motion, even in the limit of free rotation. (3) For toggling between positions at $\pm\phi$, ω_{yy} is one principal component because of mirror symmetry. (Note that 180° flips are a special case of toggling with $\phi = 90°$.) By differentiating a component in the xz plane with respect to direction, another principal component is found to lie at θ from the z axis where $\tan^2\theta = 3\cos^2\phi$. The three prinicpal com-

ponents are then $\omega_{dd} = {}^9/_8 \cos^2\theta - {}^1/_8$, $\omega_{yy} = {}^9/_8 \sin^2\theta - {}^1/_2$, and $\omega_{11} = -{}^1/_2$. The relative size of ω_{dd} and ω_{yy} changes at $\phi = 71°$. (4) For continuous rolling motion, the ring is assumed equally likely to be at any position $\phi \leq \Phi$ but, perhaps as the result of an obstruction, never to lie at an angle $\phi > \Phi$. Analysis for this situation is similar to the toggling case, but some integrations are also needed. The y axis is principal; the other principal axes lie in the xz plane at directions given by $\tan 2\theta = -8(3^{1/2})(\sin\Phi/\Phi)/(2 + 3\sin 2\Phi/\Phi)$. The principal components are $\omega_{yy} = {}^1/_{16} - {}^9/_{32}(\sin 2\Phi/\Phi)$, and $\omega_{\theta\theta} = {}^1/_{64}[-2 + 9(\sin 2\Phi/\Phi) - (\cos 2\theta)(6 + 9(\sin 2\Phi/\Phi)) + 24(3^{1/2})(\sin 2\theta)(\sin\Phi/\Phi)]$, where θ is double valued.

For methyl-group free rotors, two types of methyls must be considered. Three-fourths have two proton spins opposed to the third, and one-fourth have all protons pointing the same way. The dipolar patterns for both types are symmetric. Assuming a tetrahedral HCH bond angle and rapid rotation about the methyl C_3 axis, one methyl-group type has the same dipolar coupling as a static CH pair, while the other has only a third as strong coupling. Calculations of motionally averaged dipolar tensors are then superpositions of two CH patterns appropriately weighted, each obtained by the procedures described above.

Asymmetric Chemical Shift Anisotropy Tensors. The chemical shift anisotropy tensor in aromatic-ring carbons is asymmetric but not completely arbitrary.[28] We note that $\omega_{rr} > \omega_{tt} > \omega_{nn}$, where r stands for radial, t tangential, and n perpendicular to the ring. These components will be assumed to lie exactly along the bond symmetry axes. We will consider two kinds of C_2 rotations. (1) For 180° flips, there is no effect on the on-axis carbons. The ortho and meta carbon CSA's are altered so that the new symmetry axes are x', y', and z' and

$$\omega_{yy}' = \omega_{yy}$$

$$\omega_{zz}' = {}^3/_4\omega_{tt} + {}^1/_4\omega_{rr}$$

$$\omega_{xx}' = {}^1/_4\omega_{tt} + {}^3/_4\omega_{rr}$$

$$\mu' = \omega_{xx}' - \omega_{yy}' = \mu_0(7 + \rho_0)/8$$

$$\rho' = \frac{3 + 5\rho_0}{7 + \rho_0}$$

and

$$\rho' - \rho_0 = \frac{(3 + \rho_0)(1 - \rho_0)}{7 + \rho_0} \geq 0$$

(2) For toggling between two positions at $\pm\phi$, x, y, and z are principal axes for the on-axis carbons and

$$\omega_{zz} = \omega_{rr} = \frac{\mu_0}{2}\left(1 - \frac{\rho_0}{3}\right)$$

$$\omega_{xx} = \langle\cos^2\phi\rangle\omega_{tt} + \langle\sin^2\phi\rangle\omega_{nn} = \frac{\mu_0\rho_0}{3} - \frac{\mu_0}{2}(1 + \rho_0)\langle\sin^2\phi\rangle$$

$$\omega_{yy} = \langle\sin^2\phi\rangle\omega_{tt} + \langle\cos^2\phi\rangle\omega_{nn} = -\frac{\mu_0}{2}\left(1 + \frac{\rho_0}{3}\right) + \frac{\mu_0}{2}(1 + \rho_0)\langle\sin^2\phi\rangle$$

$$\mu' = \mu_0[1 - \langle\sin^2\phi\rangle(1 + \rho_0)/2]$$

$$\rho' = \frac{\rho_0 - 3\langle\sin^2\phi\rangle(1 + \rho_0)/2}{1 - \langle\sin^2\phi\rangle(1 + \rho_0)/2}$$

These expressions are valid for continuous rolling as well, if the appropriate average values are ϕ are used for the bracketed terms. The ortho and meta carbon CSA's are altered by toggling so that one principal component lies in the y direction, and the other two at solutions to $\tan 2\theta = 2(3^{1/2})(\cos\phi)(\rho - 1)/[\rho(\cos^2\phi - 3) + 7\cos^2\phi - 5]$. Principal components for toggling are then

$$\omega_{yy} = -\mu_0(1 + 7\cos 2\phi)/16$$

$$\omega_{aa} = \mu_0[4(3^{1/2})\sin 2\theta\cos\phi + 1 + 3\cos 2\theta + 7\cos 2\phi(1 - \cos 2\phi)]/32$$

$$\omega_{bb} = \mu_0[-4(3^{1/2})\sin 2\theta\cos\phi + 1 - 3\cos 2\theta + 7\cos 2\phi(1 + \cos 2\phi)]/32$$

Registry No. Tetrachloropolycarbonate, 26913-25-7; norbornylpolycarbonate, 24979-94-0; poly(BPA-formal), 66983-33-3; chloralpolycarbonate, 31546-39-1; polycarbonate, 24936-68-3; (tetrachloro-BPA)·(H_2CO_3) (copolymer), 26814-08-4; (4,4'-(2-norbornanylidenediphenol)·(H_2CO_3) (copolymer), 26007-14-7; (4,4'-(2,2-dichlorovinylidene)diphenol)·(H_2CO_3) (copolymer), 29057-43-0; (BPA)·(H_2CO_3) (copolymer), 25037-45-0.

References and Notes

(1) Steger, T. R.; Schaefer, J.; Stejskal, E. O.; McKay, R. A. *Macromolecules* **1980**, 13, 1127.
(2) Yee, A. F.; Smith, S. A. *Macromolecules* **1981**, *14*, 54.
(3) Schaefer, J.; McKay, R. A.; Stejskal, E. O.; Dixon, W. T. *J. Magn. Reson.* **1983**, *52*, 123.
(4) Hester, R. K.; Ackerman, J. L.; Neff, B. L.; Waugh, J. S. *Phys. Rev. Lett.* **1976**, *36*, 1081.
(5) Stoll, M. E.; Vega, A. J.; Vaughan, R. W. *J. Chem. Phys.* **1976**, *65*, 4093.
(6) Waugh, J. S.; Huber, L. M.; Haeberlen, U. *Phys. Rev. Lett.* **1968**, *20*, 180.
(7) Haeberlen, U. *Adv. Magn. Reson.* **1976**, *Suppl. 1*, 1.
(8) Munowitz, M. G.; Griffin, R. G.; Bodenhausen, G.; Huang, T. H. *J. Am. Chem. Soc.* **1981**, *103*, 2529.
(9) Munowitz, M. G.; Griffin, R. G. *J. Chem. Phys.* **1982**, *76*, 2848.
(10) Herzfeld, J.; Berger, A. E. *J. Chem. Phys.* **1980**, *73*, 6021.
(11) Cheng, V. B.; Suzukawa, H. A.; Wolfsberg, M. W. *J. Chem. Phys.* **1973**, *59*, 3992.
(12) Torchia, D. A. *J. Magn. Reson.* **1978**, *30*, 613.
(13) Opella, S. J.; Frey, M. H.; DiVerdi, J. A. *J. Magn. Reson.* **1980**, *37*, 165.
(14) Doty, F. D.; Ellis, P. D. *Rev. Sci. Instrum.* **1981**, *52*, 1868.
(15) Schaefer, J.; Stejskal, E. O.; Steger, T. R.; Sefcik, M. D.; McKay, R. A. *Macromolecules* **1980**, *13*, 1121.
(16) Schaefer, J.; Sefcik, M. D.; Stejskal, E. O.; McKay, R. A.; Dixon, W. T.; Cais, R. E. *Macromolecules* **1984**, *17*, 1105.
(17) Anderson, J. E.; Slichter, W. P. *J. Chem. Phys.* **1966**, *44*, 1797.
(18) A single-crystal X-ray analysis was performed on BPA monomer by H.-S. Shieh, Physical Sciences Center, Monsanto Co.
(19) Gall, C. M.; DiVerdi, J. A.; Opella, S. J. *J. Am. Chem. Soc.* **1981**, *103*, 5039.
(20) Kinsey, R. A.; Kintanar, A.; Oldfield, E. *J. Biol. Chem.* **1981**, *256*, 9028.
(21) Fleming, W. W.; Lyerla, J. R.; Yannoni, C. S. *Prepr. Div. Org. Coat.* **1983**, *48*, 92.
(22) Lyerla, J. R.; Yannoni, C. S. *Acc. Chem. Res.* **1982**, *15*, 208.
(23) Haeberlen, U.; Waugh, J. S. *Phys. Rev.* **1968**, *175*, 453.
(24) Abragam, A. "The Principles of Nuclear Magnetism"; Oxford University Press: London, 1961; p 565.
(25) Van Krevelen, D. W. "Properties of Polymers"; Elsevier: New York, 1976; p 267.
(26) In this paper the mean is taken of the square of the sines of the angles rather than the squares of the angles themselves to obtain a root mean square. Arcsin root mean sine square is a more accurate term. For small angles where $\sin\theta \sim \theta$, the two means are the same.
(27) Spiess, H. W. *J. Chem. Phys.* **1980**, *15*, 6755.
(28) Pausak, S.; Pines, A.; Waugh, J. S. *J. Chem. Phys.* **1973**, *59*, 591.
(29) Spiess, H. W. *Colloid Polym. Sci.* **1983**, *261*, 193.
(30) Spiess, H. W., private communication.
(31) Inglefield, P. T.; Jones, A. A.; Lubianez, R. P.; O'Gara, J. F. *Macromolecules* **1981**, *14*, 288.
(32) Inglefield, P. T.; Amici, R. M.; Hung, C.-C.; O'Gara, J. F.; Jones, A. A. Paper presented at the 24th Experimental NMR Conference, Asilomar, CA, Apr 1983, and subsequently published in *Macromolecules* **1983**, *16*, 1552.
(33) Tonelli, A. E. *Macromolecules* **1972**, *5*, 558.
(34) Tang, J.; Pines, A. *J. Chem. Phys.* **1980**, *72*, 3290.